Pulse-Width Modulation Strategy in Double-Delta Sourced Winding

Yongsoon Park and Seung-Ki Sul

Department of Electrical and Computer Engineering

Seoul National University, Seoul, Korea

Abstract—**A topology, so called, Double-Delta Sourced Winding (DDSW) has been proposed to improve harmonic properties in high-power conversion systems. In this paper, a pulse-width modulation method is proposed to further optimize the harmonic properties in DDSW-based systems. Specifically, it is described through mathematical analyses how to modify voltage references for reducing harmonics in combination with DDSW. The effectiveness of the proposed method is assessed with experimental results. As a result, the proposed method revealed 40% further reduction of harmonic current.**

I. Introduction

A circuit connection topology, so called, Double-Delta Sourced Winding (DDSW), would be useful to mitigate ripple currents by virtue of its multi-level voltage output [1]-[3]. In particular, this topology is attractive in high-power systems, where multiple windings and converters are inherently essential for power sharing [4]-[6]. It was shown in the literatures that DDSW could be feasible in power conversion systems based on a transformer or an electrical machine with dual three-phase windings. Specifically, active and reactive powers were adjusted for a grid application [2], and the vector control was achieved for a motor application [3].

In the previous literatures [1]-[3], a Pulse-Width Modulation (PWM) for DDSW was based on a simple interleaving method [1], [7]. This interleaving method uses two PWM-carriers presenting the phase difference by 180 degrees. For example, winding voltages in a DDSW-based system are shown in Fig. 1 from [1] when its PWM is based on the conventional method. In the figure, although their fundamental phases are identical, phase-shifted patterns are observed in the scope of PWM because of the interleaving. Even though the number of voltage levels is increased up to nine by DDSW [1], the employment of the voltage levels does not appear to be optimal.

A PWM output, in general, presents fluctuations with respect to its average value for a given period. These fluctuations are inevitable because voltage levels available for PWM are finite in converters. In order to mitigate PWM ripples, the magnitude of the fluctuation should be thus minimized for each PWM period. However, in the conventional PWM method, the fluctuation at the region of negative peak of fundamental voltage is much larger than that at the region of zero-crossing of fundamental voltage as shown

in Fig. 1. This fact corroborates that the PWM strategy for DDSW may be further optimized.

In this paper, after a new concept for PWM is described in a voltage vector plane, its implementation is delineated as a carrier-based scheme with mathematical analyses. The effectiveness of the proposed method is evaluated with experimental results.
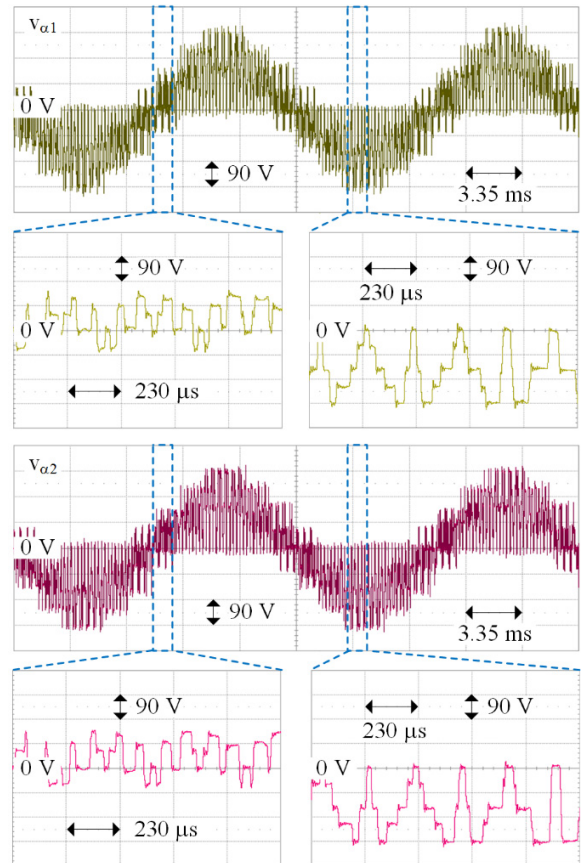
Figure 1. Winding voltage by conventional PWM in DDSW [1].

II. Voltage Synthesis in DDSW

Two converters are essential for DDSW as shown in Fig. 2. The PWM combination of these converters should be considered

for better harmonic properties not only in the converter-side but also in the other side that is magnetically coupled. In fact, the current flowing into this coupled winding is more critical in practical applications. In detail, this coupled current corresponds to a grid current of transformer or a rotor current of electrical machine. Furthermore, there are associated harmonic regulations for grid currents to comply with [8], and the degree of torque ripples is dependent on harmonics of rotor currents. Therefore, the combinational influence of converters should be more considered on the coupled winding than the converter winding.

The combinational influence of converters intuitively appears to be explained with the summation of each converter's outputs. By assuming a balanced three-phase structure in Fig. 2, a per-phase circuit can be derived as presented in Fig. 3. For simplicity, it is also assumed that L_m is large enough, and that L_p is identical to the parallel inductance of two leakage inductances, denoted by L_s, close to $v_{\alpha1}$ and $v_{\alpha2}$. The voltage drop on L_p is then derived as (1) from Fig. 3.

$$v_{\alpha p} = \frac{1}{4}(v_{\alpha1} + v_{\alpha2} - 2v_g),\qquad(1)$$

where v_g is grid voltage.

In transformer applications, because the current flowing into L_p corresponds to a grid current, the characteristics of the voltage drop detailed in (1) is important for the compliance with relevant standards [8]. When considering (1), the combinational influence of converters to the coupled winding is explained with the sum of $v_{\alpha1}$ and $v_{\alpha2}$ as expected. Therefore, the combinational influence from the converters can be extended for three-phase as (2).

$$\begin{bmatrix} v_{\alpha p\_conv} \\ v_{\beta p\_conv} \\ v_{\gamma p\_conv} \end{bmatrix} = \frac{1}{4}(\begin{bmatrix} v_{\alpha1} \\ v_{\beta1} \\ v_{\gamma1} \end{bmatrix} + \begin{bmatrix} v_{\alpha2} \\ v_{\beta2} \\ v_{\gamma2} \end{bmatrix}),\qquad(2)$$

where the grid voltages are disregarded only for considering PWM effects of the converters.

Because the winding voltages on the right-side in (2) can be expressed with respect to switching functions of each converter and DC-link voltage [1], stationary d-q voltage can be derived as (3-a) from (2) through Clarke's transformation in (3-b). Both DC-link voltages for converters are assumed to be identical as V_{dc}.

$$\begin{bmatrix} v_{dp} \\ v_{qp} \end{bmatrix} = T_c \cdot \begin{bmatrix} v_{\alpha p} \\ v_{\beta p} \\ v_{\gamma p} \end{bmatrix} = \frac{V_{dc}}{4}(A_1 \cdot \begin{bmatrix} S_a \\ S_b \\ S_c \end{bmatrix} + B_1 \cdot \begin{bmatrix} S_r \\ S_s \\ S_t \end{bmatrix}),\qquad(3\text{-}a)$$

$$T_c = \frac{2}{3}\begin{bmatrix} 1 & -1/2 & -1/2 \\ 0 & \sqrt{3}/2 & -\sqrt{3}/2 \end{bmatrix},\qquad(3\text{-}b)$$

$$A_1 = B_1 = \begin{bmatrix} 1 & -1 & 0 \\ 1/\sqrt{3} & 1/\sqrt{3} & -2/\sqrt{3} \end{bmatrix}.\qquad(3\text{-}c)$$

Given that each switching function can present unity or zero, the pairs of d-q voltage made by DDSW are indicated as finite vectors in a voltage plane as depicted in Fig. 4. Specifically, the voltage vectors from each converter in Fig. 4(a) are combined into the voltage vectors for the coupled winding in Fig. 4(b). The vector distribution in Fig. 4(b) is identical to that of a three-level converter except 30-degree rotation.
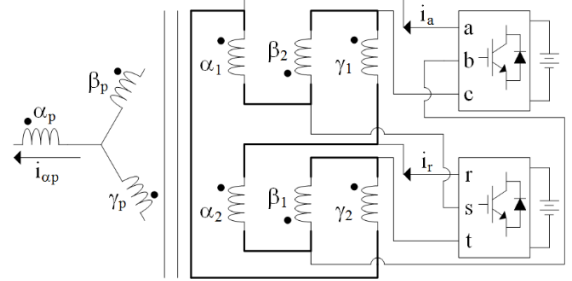
Figure 2. Winding connections for DDSW.
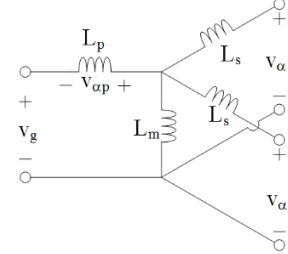
Figure 3. Per-phase equivalent circuit for DDSW.
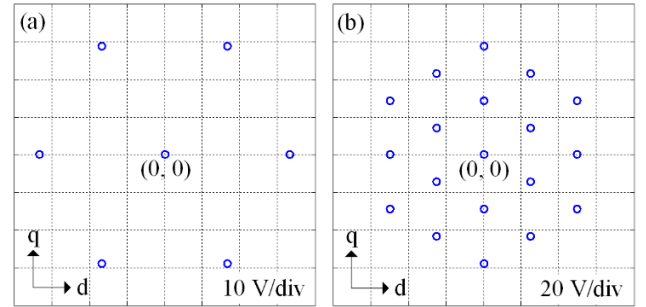
Figure 4. Position of voltage vectors by DDSW when V_{dc} is 100V in d-q plane of voltage: (a) for each converter, (b) for coupled winding.

In that the voltage vectors are distributed like a three-level converter, an optimal PWM strategy for DDSW can be similar to that for open-end winding [9], [10]. However, in the open-end winding case, two converters forcibly share identical converter currents due to its structure. Namely, as only one three-phase current is of concern to determine six switching functions, two converters for the open-end winding can be regarded as one three-level converter if their DC-link voltages are equal. On the contrary, different three-phase currents can flow in each converter of DDSW-based systems. That is, separate current regulators are normally dedicated to each converter [2], [3]. Furthermore, it

should be noted that the coefficients for each voltage in (1) are actually dependent on intermediate impedances of a DDSW-based system. Strictly speaking, the purpose of PWM for DDSW is then aimed at quasi three-level operations. In the proposed method, after two sets of three-phase voltage references are initially computed for the current regulation of each converter, they are aptly modified for the quasi three-level operation without deteriorating the current regulations.

The conventional PWM for DDSW can be understood with an example shown in Fig. 5. Normally, almost identical reference vectors are assigned to both converters, CNV_1 and CNV_2, for the current regulations. However, the appearing sequences of voltage vectors to synthesize the reference vectors are opposite in each converter due to the interleaving effect as shown in Figs. 5(b) and 5(c). As a result, in synthesizing the combined reference vector 'R', three voltage vectors indicated by circles are used for PWM in the combined voltage plane as shown in Fig. 5(a). That is, when the conventional PWM is employed, the nearest surrounding vectors to the combined reference vector may not be used for voltage synthesis, which is detrimental to harmonic properties.

For better harmonic properties, each converter should employ only the nearest surrounding vectors for the voltage synthesis. One example is shown in Fig. 6 to explain the principle of the proposed method. In here, one converter is used to maintain a pivot vector as shown in Fig. 6(b) while the other converter generates enclosing vectors as presented in Fig. 6(c). The combined reference vector 'R' can then be synthesized with only the nearest surrounding vectors as indicated by circles in Fig. 6(a). By alternately exchanging the roles of each converter, the proposed PWM method can be applied without degrading the current regulations.

III.   REFERENCE MODIFICATION IN PROPOSED PWM

A. Fundamental Concepts to Explain Proposed Method

Several concepts need to be mentioned before explaining the proposed method. In general, voltage vectors in a two-level converter form a hexagon [11], [12]. If the magnitude of a voltage vector is not null, it is referred to as effective vector, and only one combination of switching functions is matched to it as shown in Fig. 7. In this paper, if only one of switching functions presents unity for an effective vector, it is denoted by single-one vector (SOV). On the contrary, if only one of switching functions presents zero, it is represented by single-zero vector (SZV). As shown in Fig. 7, every sector of the hexagon (S1~S6) is separated by a SOV and a SZV. Therefore, the principle of PWMs can be explained in terms of SOV and SZV regardless of the actual sector which a reference vector belongs to.

A space vector modulation (SVM) for a three-phase reference can be easily carried out by using a triangular waveform as shown in Fig. 8 [13], where only the half period for PWM, represented by T_{samp}, is presented. Simply, if a voltage reference is higher than the triangular-wave in real time, its switching function presents unity. Otherwise, the value of switching function corresponds to zero. In fact, SVM intended in Fig. 8 is mathematically based on (4) [12].

$$\vec{V}^* = \frac{1}{T_{samp}} (\vec{V}_{sov} \cdot T_{sov} + \vec{V}_{szv} \cdot T_{szv}) . \qquad (4)$$

As mentioned earlier, because every sector is bounded by a SOV and a SZV, each effective vector is indicated by SOV or SZV as its subscript in (4).
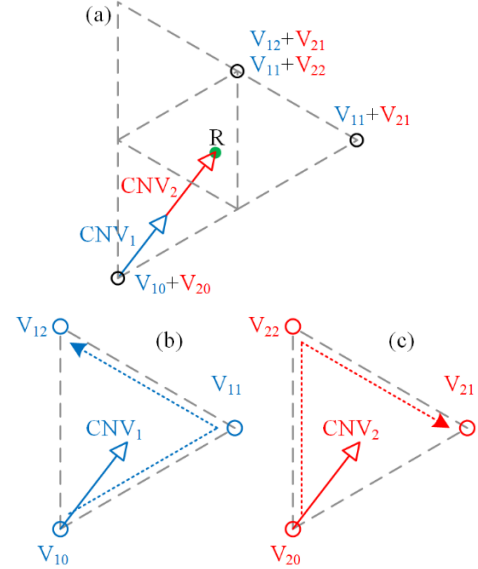
Figure 5. Employment of voltage vectors in conventional PWM.
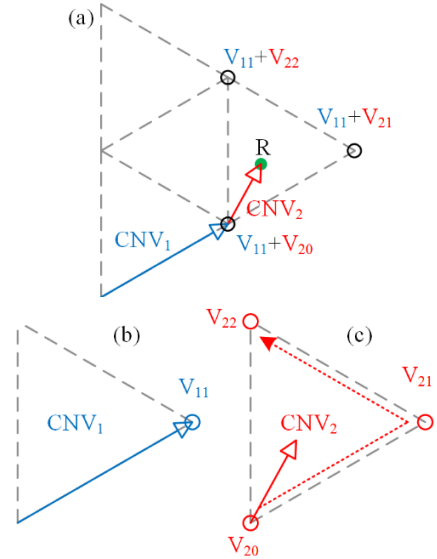
Figure 6. Employment of voltage vectors in proposed PWM.

If each voltage reference is classified as V_{max}, V_{med}, and V_{min} according to its relative magnitude to the others, the analysis on PWM can be further generalized. In Fig. 8, voltage differences of a three-phase reference are proportional to the application times of effective vectors due to the linearly changed slope of the

triangular-wave. Specifically, the difference between V_{max} and V_{med} is related to the application time of SOV while the difference between V_{med} and V_{min} is associated with the application time of SZV. This is because only one switching function presents unity if and only if V_{max} is solely higher than the triangular-wave, and only one switching functions presents zero if and only if V_{min} is exclusively lower than the triangular-wave. Therefore, (4) can be rearranged into (5) when it comes to the generalized voltage references.
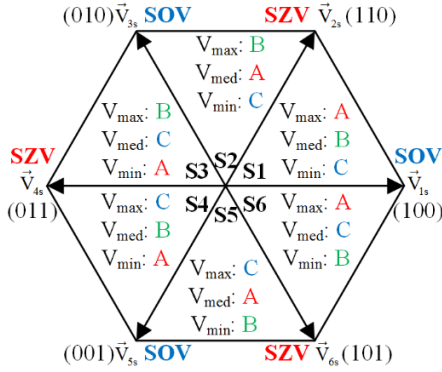
Figure 7. Definition of voltage vectors for two-level converter.
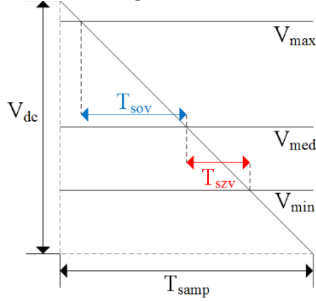
Figure 8. PWM based on a triangular waveform.

$$\vec{V}^* = \frac{1}{T_{samp}} \cdot \frac{T_{samp}}{V_{dc}} \cdot \{\vec{V}_{sov} \cdot (V_{max} - V_{med}) + \vec{V}_{szv} \cdot (V_{med} - V_{min})\} . \qquad (5)$$

The meaning of (5) is that a three-phase reference voltage for the current regulation can be synthesized during T_{samp} with a triangular-wave having the slope of V_{dc}/T_{samp}. On the basis of the aforementioned concepts, it is detailed how the proposed method is implemented.

B. Carrier-Based Implmenetation for Proposed Method

As mentioned earlier, each converter has to alternately change its role for the proposed PWM: pivoting mode and enclosing mode. In addition, because PWM period for the current regulation is given as T_{samp}, the role change must be made within T_{samp} not to degrade the current regulation. The equal time for each mode, as presented in (6), appears to be reasonable given that symmetrical PWMs are commonly good for better harmonic properties.

$$T_{pivot} = T_{enclosing} = T_{samp} / 2 . \qquad (6)$$

If T_{pivot} in (6) is inserted into (5) to substitute with T_{samp}, (7) can be derived.

$$\vec{V}^* = \frac{1}{2T_{pivot}} \cdot \frac{T_{pivot}}{V_{dc}} \cdot \{\vec{V}_{sov}(V_{maxs} - V_{meds}) + \vec{V}_{szv}(V_{meds} - V_{mins})\} ,$$

$$(7\text{-}a)$$

$$V_{maxs} = 2V_{max} , \ V_{meds} = 2V_{med} , \ V_{mins} = 2V_{min} . \qquad (7\text{-}b)$$

When compared to (5), it is inferred from (7) that a three-phase voltage in (7-b) can be synthesized during $2T_{pivot}$ with a triangular-wave having the slope of V_{dc}/T_{pivot}. Based on this insight, carrier waves in Fig. 9 would be used for the proposed PWM when considering the symmetry. In particular, as described in (7-b), the voltage references to be synthesized during $2T_{pivot}$ are two times to the initial voltage references in each converter. For the proposed PWM, these doubled references should be split into two sets of three-phase references, which are respectively utilized in pivoting mode and enclosing mode.
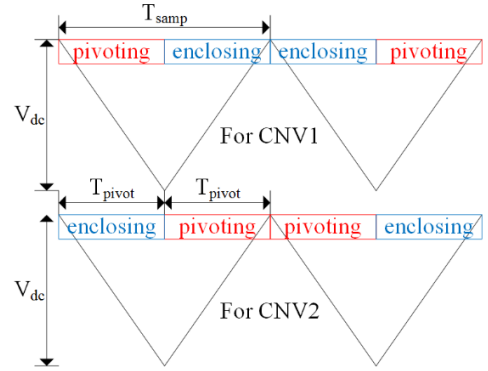
Figure 9. PWM based on a triangular waveform.

Equation (7) needs to be modified for a carrier-based PWM when considering the relationship between Fig. 8 and (5). That is, (5) is given for a carrier-based PWM during the half period of the carrier. Therefore, given that (7-a) is given for $2T_{pivot}$, which is the full period of the triangular-wave in Fig. 9, equation (7) can be modified into (8) for each converter.

$$\vec{V}^* = \frac{1}{2T_{pivot}} \frac{T_{pivot}}{V_{dc}} \{\vec{V}_{sov1}(V_{max1} - V_{med1}) + \vec{V}_{szv1}(V_{med1} - V_{min1})$$

$$+ \vec{V}_{sov2}(V_{max2} - V_{med2}) + \vec{V}_{szv2}(V_{med2} - V_{min2})\} \qquad (8)$$

where V_{max1}, V_{med1}, and V_{min1} are modified references for pivoting mode, and V_{max2}, V_{med2}, and V_{min2} for enclosing mode. In addition, SOV and SZV for each mode in (8) may be different with those in (7-a).

C. Reference Modification by Proposed Method

It is now explained how to derive the modified references in (8) from the original references in (7-b). The combined voltage plane in Fig. 4(b) can be divided into sub-sectors as shown in Fig. 10 for a 60-degree range. These sectors can be distinguished by some conditions with respect to the original references.
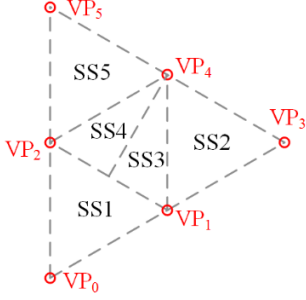
Figure 10. Sector division in the combined plane.

i) $V_{maxs} - V_{mins} < V_{dc}$ (SS1)

This condition actually means that the summation of $(V_{maxs}-V_{meds})$ and $(V_{meds}-V_{mins})$ is smaller than V_{dc}. If this summation is multiplied by T_{pivot}/V_{dc} according to (7), it corresponds the total application time of effective vectors. Therefore, the total application time is smaller than T_{pivot} under this condition, and a combined reference vector can be synthesized within the half period of the triangular-wave in Fig. 9. This fact indicates that zero vectors, VP_0 in Fig. 10, can be used as a pivot vector because the combined reference vector is located in SS1.

A modification can be made in (7) to derive (9) with the addition of zeros, which is numerically meaningless.

$$\vec{V}^* = \frac{1}{2T_{pivot}} \frac{T_{pivot}}{V_{dc}} \{ \vec{V}_{sov} \cdot (V_{maxs} + 0 - V_{meds}) + \vec{V}_{szv} \cdot (V_{meds} + 0 - V_{mins}) \} . \qquad (9)$$

Equation (9) is then rearranged into (10) that has exactly the same format with (8).

$$\vec{V}^* = \frac{1}{2T_{pivot}} \frac{T_{pivot}}{V_{dc}} \{ \vec{V}_{sov} \cdot 0 + \vec{V}_{szv} \cdot 0 + \vec{V}_{sov}(V_{maxs} - V_{meds}) + \vec{V}_{szv}(V_{meds} - V_{mins}) \} . \qquad (10)$$

When comparing (8) and (10), the voltage differences, which are proportional to the application times for SOV and SZV, are derived as (11) for each mode.

$$\begin{cases} V_{max1} - V_{med1} = 0 \\ V_{med1} - V_{min1} = 0 \end{cases}, \qquad (11\text{-}a)$$

$$\begin{cases} V_{max2} - V_{med2} = V_{maxs} - V_{meds} \\ V_{med2} - V_{min2} = V_{meds} - V_{mins} \end{cases} . \qquad (11\text{-}b)$$

Two points are inferred from (10) and (11) for this sector. Firstly, SOV and SZV are not changed by the proposed method. Secondly, values of three-phase references are specified by adding zero-sequence voltages because the voltage differences are only given in (11). For example, three-phase references for each mode in SS1 are derived as (12) when the initial phases of V_{max}, V_{med}, V_{min} in (7) are assumed to be a, b, and c, respectively. In addition, zero-sequence voltages can be determined such that all of three-phase references intersect with the carrier wave unless the converter is under over-modulation.

$$\begin{cases} V_{a\_pivot} = V_{zs1} \\ V_{b\_pivot} = V_{zs1} \\ V_{c\_pivot} = V_{zs1} \end{cases}, \qquad (12\text{-}a)$$

$$\begin{cases} V_{a\_enclosing} = V_{maxs} + V_{zs2} \\ V_{b\_enclosing} = V_{meds} + V_{zs2} \\ V_{c\_enclosing} = V_{mins} + V_{zs2} \end{cases}, \qquad (12\text{-}b)$$

where V_{zs1} and V_{zs2} are zero-sequence voltages and should be carefully determined because they can affect the switching frequency of each converter.

As shown in Fig. 9, when one converter is in pivoting mode, the other converter is in enclosing mode. Therefore, if the references according to (12-a) are used for PWM in one converter, the references according to (12-b) are simultaneously used for PWM in the other converter. In each converter, the three-phase references by (12-a) and (12-b) have to be computed at once per T_{samp} for pivoting mode and enclosing mode, respectively.

In the remaining sectors, $V_{maxs}-V_{mins}$ is larger than or equal to V_{dc} even if it is not explicitly mentioned. In addition, pivot vectors in those sectors must be VP_1 or VP_2 under the consideration of vector summations in Fig. 10 because the magnitude of pivot vectors must be synthesized by a single converter during T_{pivot}.

ii) $V_{maxs} - V_{meds} \geq V_{meds} - V_{mins}$ (SS2 or SS3)

This condition indicates that the application time of a SOV is larger than or equal to that of a SZV, which is corroborated with the earlier explanations, related to Fig. 8 and (4). Therefore, a combined reference vector from (7-b) is closer to the SOV than the SZV. For example, in Fig. 10, as VP_1 corresponds to the SOV, the combined reference vector is located in SS2 or SS3. A pivot vector should be geometrically close to a combined reference vector in order to employ the nearest surrounding vectors for PWM. Therefore, under this condition, a SOV should be selected as a pivot vector. In order to apply the SOV as the pivot vector, one reference voltage has to be greater than the other reference

voltages by V_{dc} during the whole pivoting period. This assignment for pivoting mode can be derived according to (13), which is numerically equal to (7).

$$\vec{V}^* = \frac{1}{2T_{pivot}} \frac{T_{pivot}}{V_{dc}} \{ \vec{V}_{sov} \cdot (V_{maxs} + V_{dc} - V_{dc} - V_{meds})$$
$$+ \vec{V}_{szv} \cdot (V_{meds} + 0 - 0 - V_{mins}) \} \tag{13}$$

By simply rearranging (13), equation (14) can be derived, matched to (8).

$$\vec{V}^* = \frac{1}{2T_{pivot}} \frac{T_{pivot}}{V_{dc}} [\vec{V}_{sov} \cdot V_{dc} + \vec{V}_{szv} \cdot 0$$
$$+ \vec{V}_{sov} \{(V_{maxs} - V_{dc}) - V_{meds}\} + \vec{V}_{szv}(V_{meds} - V_{mins})] \tag{14}$$

By assigning the pivot vector, the enclosing vectors are automatically computed as shown in (14). In particular, the sign of $V_{maxs} - V_{dc} - V_{meds}$ determines whether the combined reference vector belongs to SS2 or SS3. If it is positive, the corresponding sector is SS2, and the SOV and SZV in (7) is identically used for each mode. Otherwise, the SOV in enclosing mode is changed by another SOV, denoted by $\vec{V}_{sov\_n}$ in (15). From the perspective of Fig. 7, the new SOV and the original SOV are symmetrical to the original SZV. This case is described with (15), which is numerically identical to (14).

$$\vec{V}^* = \frac{1}{2T_{pivot}} \frac{T_{pivot}}{V_{dc}} [\vec{V}_{sov} \cdot V_{dc} + \vec{V}_{szv} \cdot 0$$
$$+ \vec{V}_{sov\_n} \{V_{meds} - (V_{maxs} - V_{dc})\} + \vec{V}_{szv} \{(V_{maxs} - V_{dc}) - V_{mins}\}] \tag{15}$$

As shown in (14) and (15), if a combined reference vector is close to a SOV, V_{maxs} is subtracted by V_{dc} in enclosing mode to compensate for the usage of SOV as a pivot vector. Just the relative magnitudes among three phases are changed in (15) on contrary to (14). If three-phase references are obtained by adding zero-sequence voltages from (14) or (15), no difference is observed for the proposed PWMs in SS2 and SS3 as presented in (16), where three-phase references for each mode are derived under the same assumption with (12) in terms of phase sequences.

$$\begin{cases} V_{a\_pivot} = V_{dc} + V_{zs1} \\ V_{b\_pivot} = V_{zs1} \\ V_{c\_pivot} = V_{zs1} \end{cases}, \tag{16-a}$$

$$\begin{cases} V_{a\_enclosing} = V_{maxs} - V_{dc} + V_{zs2} \\ V_{b\_enclosing} = V_{meds} + V_{zs2} \\ V_{c\_enclosing} = V_{mins} + V_{zs2} \end{cases}. \tag{16-b}$$

iii) $V_{maxs} - V_{meds} < V_{meds} - V_{mins}$ (SS4 or SS5)

This condition indicates that the application time of a SZV is larger than that of a SOV, and a combined reference vector from (7-b) is closer to the SZV than the SOV. For instance, in Fig. 10, given that VP_2 corresponds to the SZV, the combined reference vector is located in SS4 or SS5. A SZV is thus selected as a pivot vector under this condition, and V_{mins} is added by V_{dc} in enclosing mode to compensate for the usage of SZV as a pivot vector. Under the identical assumption to (16), three-phase references for each mode are then derived as (17).

$$\begin{cases} V_{a\_pivot} = V_{zs1} \\ V_{b\_pivot} = V_{zs1} \\ V_{c\_pivot} = -V_{dc} + V_{zs1} \end{cases}, \tag{17-a}$$

$$\begin{cases} V_{a\_enclosing} = V_{maxs} + V_{zs2} \\ V_{b\_enclosing} = V_{meds} + V_{zs2} \\ V_{c\_enclosing} = V_{mins} + V_{dc} + V_{zs2} \end{cases}. \tag{17-b}$$

Finally, the reference modification by the proposed PWM method for each converter can be summarized with the examples of (12), (16), and (17), where the initial phases of V_{max}, V_{med}, V_{min} are assumed to be a, b, and c, respectively. For practical utilization, depending on the reference voltage conditions, the identical procedures have only to be applied for a three-phase reference after the initial phases of V_{max}, V_{med}, V_{min} are detected.

In fact, a switching frequency of the proposed method can be altered by how to set zero-sequence voltages in pivoting mode and enclosing mode. The relevant discussion is very important, but it is not the scope of this paper. Instead, it is notified that the total number of switching instants for three phases per $2T_{samp}$ was smaller than or equal to six in the following experimental results by the proposed method. Under the consideration of the switching frequency according to Fig. 8 for T_{samp}, this criterion means that the switching frequency of the proposed method was identical to that of the conventional method.

IV. EXPERIMENTAL RESULTS

The proposed method was tested in two experimental systems. At first, two-level converters for DDSW were composed of 600V-75A intelligent power modules as shown in Fig. 11. Their control algorithms were fully implemented with a DSP board based on TMS320C28346. With these converters, two DDSW-based PWM systems were tested, namely, a 6-kVA transformer system with two sets of three-phase secondary windings in Fig. 12 and an 11-kW induction machine drive system with two sets of three-phase stator windings in Fig. 13.

Initially, the proposed method was compared with the conventional method in the transformer system. The switching frequency was 2.5 kHz for both PWM methods to emulate a high-

power system, and the DC-link voltages were set to 260 V when the transformer was connected to an 110V-60Hz grid. This test set-up was considered for a battery energy storage system whose battery is fully charged, and the modulation index (MI) to $V_{dc}/\sqrt{3}$ was 0.67 V/V. When the rated current flew into the grid, winding voltages by each method were shown in Fig. 14.

Figure 11. Two-level converters for DDSW.

Figure 12. 6 kVA DDSW-based transformer.

Figure 13. Test set-up for 11 kW DDSW-based induction machine.

Nine levels are used to synthesize the winding voltages in the DDSW system by both PWM methods. However, because PWM was modified by the proposed method to utilize only the nearest surrounding vectors, its effect could be confirmed with the mitigation of current ripples as shown in Fig. 15. When the fundamental of the grid current i_{ag} was about 43 A, its Total Harmonic Distortion (THD) was decreased by the proposed method from 13.4 % to 7.6 %. In addition, when the fundamental of the converter current i_a was about 22 A, its THD was decreased by the proposed method from 13.4 % to 8.3 %. From these results,

it can be noted that ripple currents has been reduced by virtue of the proposed method not only in the coupled winding but also in the converter-side winding.
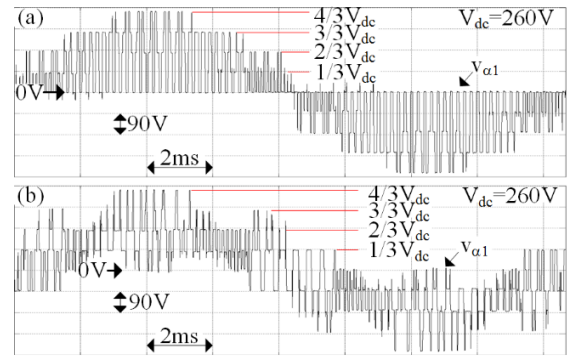
Figure 14. Winding voltages in DDSW-based transformer: (a) conventional PWM method, (b) proposed PWM method.
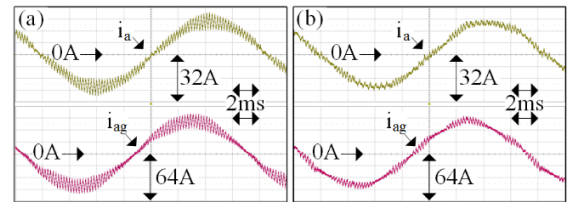
Figure 15. Converter current and grid current in DDSW-based transformer: (a) conventional PWM method, (b) proposed PWM method.

The harmonic properties depending on MI can be evidently observed in the DDSW-based system for the induction machine. For the induction machine drives, the DC-link voltages were set to 315 V, and the switching frequency was 1.25 kHz. While the MI cannot be lowered under a certain value in the transformer application due to the grid voltage, wide variation of MI is possible by the speed control in the induction machine drives because the back Electromotive Force (EMF) is proportional to the speed. When the induction machine was driven with no load by the V/f control at 20, 40, and 60 Hz, the winding voltages by each method were presented in Figs. 16 and 17.

The merits of the proposed method are more obvious at low and high MIs. Firstly, when MI was 0.33, the maximum level used for the voltage synthesis was $2/3 \cdot V_{dc}$ in the proposed method while that was $4/3 \cdot V_{dc}$ in the conventional method. That is, in the voltage synthesis, PWM fluctuations from an average voltage during a switching period could be minimized by the proposed method. This also corroborates that the voltage variation of windings (dv/dt) can be kept low by the proposed method, which is good for mitigating leakage currents in high-power systems. Secondly, when MI was 0.99, the winding voltage could become closer to a sine-wave by the proposed method. Specifically, when the fundamental magnitude was at its peak, the zero-potential was still used for the voltage synthesis in the conventional method while it does not at all in the proposed method. Through the overall MI range, it can be recognized that, in the view point of the PWM

fluctuations, the proposed method would be better than the conventional method.
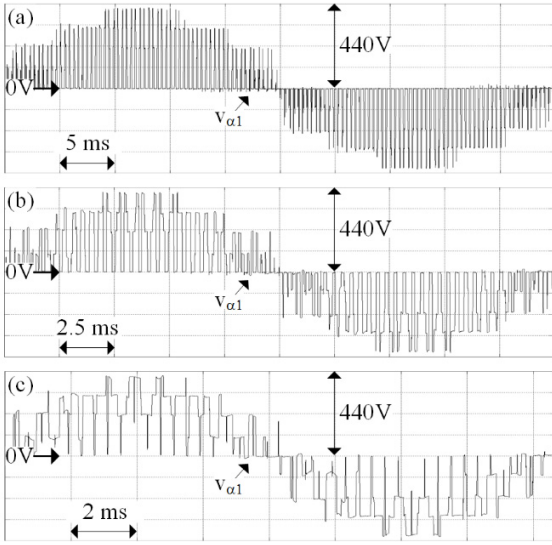
Figure 16. Winding voltages by conventional PWM for the induction machine: when MI is (a) 0.33, (b) 0.66, (c) 0.99.
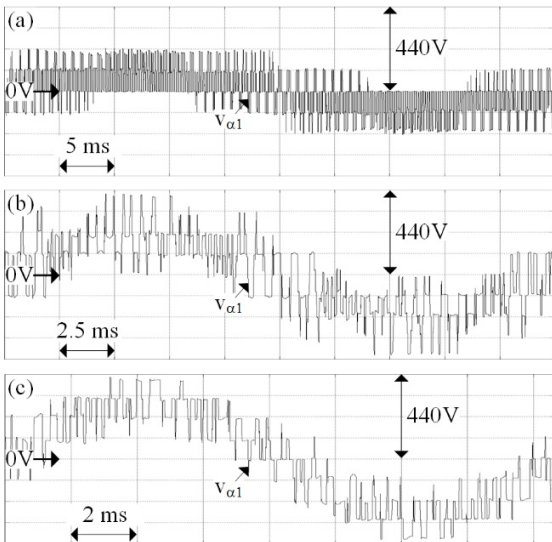
Figure 17. Winding voltages by proposed PWM for the induction machine: when MI is (a) 0.33, (b) 0.66, (c) 0.99.

V. CONCLUSION

In this paper, a PWM method has been proposed to achieve quasi three-level operations for the systems based on double-delta sourced winding. The proposed method is easily implemented with carrier-waves, and its principle to modify the voltage references for the current regulation has been mathematically discussed. The effectiveness of the proposed method has been validated with experimental results based on two different systems, a transformer with two sets of secondary windings, and an induction motor with two sets of stator windings. It has been shown that current ripples has been reduced by 40% through the proposed PWM method.

REFERENCES

[1] Y. Park, S. Ohn, and S.-K. Sul, "Multi-Level Operation with Two-Level Converters Through a Double-Delta Source Connected Transformer," *Journal of Power Electron.*, vol. 14, no. 6, pp. 1093-1099, Nov. 2014.

[2] Y. Park, J.-M. Yoo, and S.-K. Sul, "Current regulation and fault tolerance in Double-Delta Sourced Transformer," *2015 IEEE Energy Conversion Congress and Exposition (ECCE)*, Montreal, QC, 2015, pp. 1541-1548.

[3] Y. Park, J.-M. Yoo, and S.-K. Sul, "Double-delta sourced winding for dual winding induction machine," *2015 9th International Conference on Power Electronics and ECCE Asia (ICPE-ECCE Asia)*, Seoul, 2015, pp. 77-85.

[4] S. Brisset, D. Vizireanu, and P. Brochet, "Design and Optimization of a Nine-Phase Axial-Flux PM Synchronous Generator with Concentrated Winding for Direct-Drive Wind Turbine," *IEEE Trans. Ind. Appl.*, vol. 44, pp. 707-715, 2008.

[5] F. B. Grigoletto and H. Pinheiro, "Flexible Arrangement of Static Converters for Grid-Connected Wind Energy Conversion Systems," *IEEE Trans. Ind. Electron.*, vol. 61, pp. 4707-4721, 2014.

[6] E. Cengelci, P. N. Enjeti, and J. W. Gray, "A new modular motor-modular inverter concept for medium-voltage adjustable-speed-drive systems," *IEEE Trans. Ind. Appl.*, vol. 36, pp. 786-796, 2000.

[7] S. Schroder, P. Tenca, T. Geyer, P. Soldi, L. J. Carces, R. Zhang, T. Toma, and P. Bordignon, "Modular High-Power Shunt-Interleaved Drive System: A Realization up to 35 MW for Oil and Gas Applications," *IEEE Trans. Ind. Appl.*, vol. 46, no. 2, pp. 821-830, Mar./April 2010.

[8] *IEEE Standard for Interconnecting Distributed Resources With Electric Power Systems*, IEEE Std. 1547, 2003.

[9] D. Casadei, G. Grandi, A. Lega, and C. Rossi, "Multilevel Operation and Input Power Balancing for a Dual Two-Level Inverter with Insulated DC Sources," *IEEE Trans. Ind. Appl.*, vol. 44, no. 6, Nov./Dec. 2008.

[10] G. Grandi, C. Rossi, D. Ostojic, and D. Casadei, "A New Multilevel Conversion Structure for Grid-Connected PV Applications," *IEEE Trans. Ind. Electron.*, vol. 56, no. 11, Nov. 2009.

[11] J. Holtz, W. Lotzkat, and A.M. Khambadkone, "On Continuous Control of PWM Inverters in the Overmodulation range including the six-step mode," *IEEE Trans. Power Electron.*, vol. 8, no. 4, pp. 546-553, Oct. 1993.

[12] Y. Park, S. K. Sul and K. N. Hong, "Linear Overmodulation Strategy for Current Control in Photovoltaic Inverter," *IEEE Trans. Ind. Appl.*, vol. 52, no. 1, pp. 322-331, Jan.-Feb. 2016.

[13] Dae-Woong Chung, Joohn-Sheok Kim and Seung-Ki Sul, "Unified voltage modulation technique for real-time three-phase power conversion," *IEEE Trans. Ind. Appl.*, vol. 34, no. 2, pp. 374-380, Mar/Apr 1998.